Carbon 154 (2019) 238–243

Contents lists available at ScienceDirect

Carbon

journal homepage: www.elsevier.com/locate/carbon

Conductance interference effects in an electron-beam-resist-free chemical vapor deposition graphene device sandwiched between two h-BN sheets

Chiashain Chuang [a], Masaaki Mineharu [b], Masahiro Matsunaga [b, c], Chieh-Wen Liu [d, e], Bi-Yi Wu [e], Gil-Ho Kim [f], Kenji Watanabe [g], Takashi Taniguchi [g], Chi-Te Liang [e, *], Nobuyuki Aoki [b, **]

[a] Department of Electronic Engineering, Chung Yuan Christian University, Taoyuan, 320, Taiwan
[b] Department of Materials Science, Chiba University, Chiba, 263-8522, Japan
[c] Venture Business Laboratory, Nagoya University, Nagoya, 464-8601, Japan
[d] Department of Physics, Case Western Reserve University, 2076 Adelber Road, Cleveland, OH, 44106, USA
[e] Graduate Institute of Applied Physics, National Taiwan University, Taipei, 106, Taiwan
[f] School of Electronic and Electrical Engineering and Sungkyunkwan Advanced Institute of Nanotechnology (SAINT), Sungkyunkwan University, Suwon, 16419, South Korea
[g] Advanced Materials Laboratory, National Institute for Materials Science, 1-1 Namki, Tsukuba, 305-0044, Japan

ARTICLE INFO

Article history:
Received 24 April 2019
Received in revised form
24 June 2019
Accepted 17 July 2019
Available online 25 July 2019

Keywords:
Graphene
Chemical vapor deposition
Boron nitride
Coherent
Interference

ABSTRACT

We report fabrication and measurements of hexagonal boron nitride (*h*-BN)/chemical vapor deposition (CVD) graphene/*h*-BN heterostructure devices without using expensive, time-consuming electron-beam lithography and toxic carbon tetrafluoride or sulfur tetrafluoride etching. We use efficient transfer of *h*-BN/CVD graphene by polypropylene carbonate onto a pre-prepared metal contacts/*h*-BN/SiO_2 substrate. In this case, CVD-graphene is suspended from the *h*-BN substrate which allows efficient gas annealing process for improving the device mobility. Interestingly, we find that the top *h*-BN capping layer could enhance the carrier interference effect in CVD graphene, a great advantage for low-cost graphene-based interference-type electronic devices.

© 2019 Elsevier Ltd. All rights reserved.

1. Introduction

In order to achieve commerical realization of electronic applications for graphene, chemical vapor depositon (CVD) growth is a promising route to scalable, low-cost and controllable method for mass production of graphene-based devices [1–5]. Importantly, hexagonal boron nitride (*h*-BN) with an almost perfect lattice match with graphene and a large band gap (5.2–5.4 eV) can provide a good dielectric material for CVD graphene so as to improve the transport mobility and enhance screening from impurities [6–8]. Although intrinsic grain boundaries, merged domains and impurities may exist in CVD graphene during the growth processes which cause the lower mobility in comparision with that of exfoliated graphene [9]. Recently *h*-BN encapsulated CVD graphene can have a transport mobility which is close to that of exfoliated graphene [10–13]. This suggests that CVD graphene may find possible device applications in ballistic transport for novel nano-electronic devices such as ballistic graphene nanoribbons [14], Veselago lenses [15], Klein tunneling transistors [16] and ballistic rectifiers [17], which is based on the fundmental principles in electron optics [15,17–20].

Although *h*-BN/graphene-based devices have the aforementioned advantages for practical device applications, electron-beam lithography-related processes for *h*-BN/exfoliated graphene/*h*-BN etching for preparing one-dimensional edge contacts [7] by toxic carbon tetrafluoride (CF_4) or sulfur tetrafluoride (SF_4) (Ref. 12) plasma etching are high-cost and time-consuming. In order to

* Corresponding author.
** Corresponding author.
E-mail addresses: ctliang@phys.ntu.edu.tw (C.-T. Liang), n-aoki@faculty.chiba-u.jp (N. Aoki).

https://doi.org/10.1016/j.carbon.2019.07.057
0008-6223/© 2019 Elsevier Ltd. All rights reserved.

fabricate *h*-BN/CVD graphene/*h*-BN high mobility sandwiched devices for industrial productions, it is highly desirable to prepare such devices using optical lithography-related processes in micrometer scale without using e-beam lithography-related processes as well as toxic CF_4 or SF_4 plasma etching. On the other hand, the interference effect possibly due to intrinstic grain boundaries and merged domains on CVD graphene with SiO_2 substrate recently have been studied by low-temperature scanning gate microscopy [21–23], which provides a possible path toward future quantum interference nano-electronic transistor for information technology [24]. Therefore it is natural to see whether the *h*-BN encapsulated CVD graphene device is better for probing coherent transport in comparision with graphene on a SiO_2 substrate. Recently we found large linear magnetoresistance and heat diffusion effect behaviors in top *h*-BN/CVD graphene devices [25,26], but there are no related studies about interference-type *h*-BN/CVD graphene/*h*-BN electronic devices. In this paper, we demonstrate how to fabricate e-beam-resist-free interference-type *h*-BN/CVD graphene/*h*-BN electronic devices and perform transport measurements on these devices at room temperature and at low temperatures. The magnitude of conductance oscillations in *h*-BN epcapsulated CVD graphene is one order magnitude larger than that in graphene on a SiO_2 substrate. The *h*-BN/exfoliated graphene/*h*-BN device also keeps high mobility transport property [27,28], and maintains the same magnitude of conductance oscillations in comparision with *h*-BN/CVD graphene/*h*-BN device due to the encapsulated *h*-BN layer. Our experimental results provide a step towards industrial applications in CVD graphene-based interference-type electronic devices.

2. Experimental

The illustration of the *h*-BN/CVD graphene/*h*-BN device fabrication is shown in Fig. 1. The high purity and homogeneous *h*-BN crystals were synthesized by the high pressure techniques [29]. We used the scotch tape method to mechanically exfoliate *h*-BN and pasted them on a 300-nm-thick SiO_2 substrate [6,30]. 10–50 nm-thick flat *h*-BN flakes [6], which were confrimed by atomic force microscope, were searched and we deposit 5 nm Cr (or Ti)/15–50 nm Au which serve as Ohmic contacts for the graphene device. The *h*-BN/SiO_2 substrate serves as a dielectric material for graphene [31] instead of just a SiO_2 substrate as shown in Fig. 2 (a). In order to maintain the CVD graphene film quality and reduce the tape residues, Gel-Pak polymer was used to transfer *h*-BN flakes

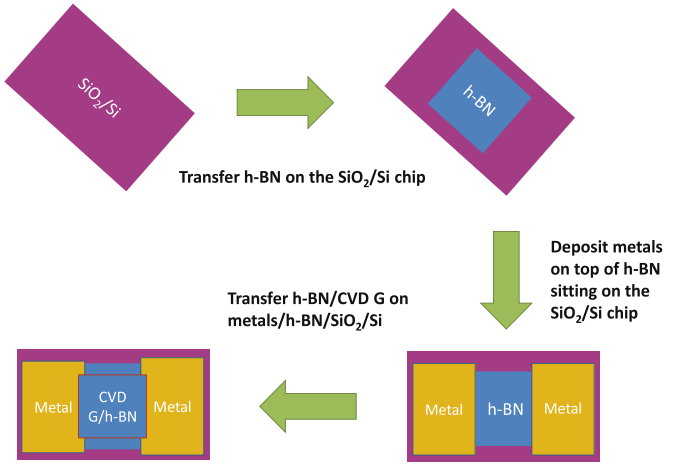

Fig. 1. Schematic diagrams showing the procedure for fabrication of an *h*-BN/CVD graphene/*h*-BN device. (A colour version of this figure can be viewed online.)

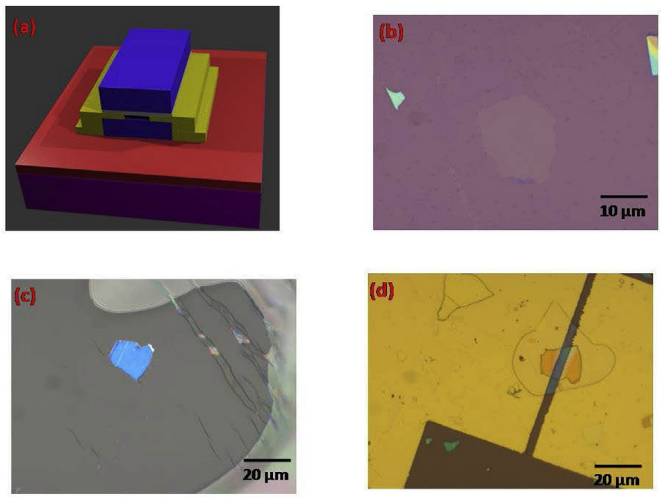

Fig. 2. (a) Schematic illustration of *h*-BN/CVD graphene/*h*-BN device. From top to bottom: *h*-BN, CVD graphene, metal contacts (Titanium (Ti)/Gold (Au) or Chromium (Cr)/Gold (Au)), *h*-BN, silicon dioxide and silicon. (b) The CVD graphene void after transferring the *h*-BN/CVD graphene flake. The scale bar is 10 μm. (c) The *h*-BN/CVD graphene flake on PPC/Gel-Pak polymer. The scale bar is 20 μm. (d) The top view of *h*-BN/CVD graphene/*h*-BN device after transferring the *h*-BN/CVD graphene onto metal contacts which were pre-deposited on the bottom *h*-BN layer. The scale bar is 20 μm. (A colour version of this figure can be viewed online.)

that located on the SiO_2 substrate onto CVD graphene/SiO_2 due to the viscoelastic effect. The commerical single layer CVD graphene contains 10–30% bilayer islands due to the low-cost and effective productions for matching our industrial application regimes on a SiO_2 substrate [32,33]. Liquid polypropylene carbonate (PPC) was dropped fully on *h*-BN/CVD graphene/SiO_2 chip and baked on hot platform at 90 C for 5 min in order to form solid thin film on the chip, which is an effective route to attach *h*-BN/CVD graphene on a substrate that is different from the traditional dry transferred method [7]. After that, we used a pair of tweezers to take the PPC solid film attached *h*-BN/CVD graphene. This approach leaves a void of the CVD graphene after removing the film as shown in Fig. 2 (b). We then flip the PPC/*h*-BN/CVD graphene composite onto the Gel-Pak polymer/slide glass as shown in Fig. 2 (c). Subsequently we transfer it to the bottom *h*-BN with metal contacts, which were defined by conventional optical lithography, metal evaporation, and lift-off process, by our 2D material transferring manipulator [7] as shown in Fig. 2 (a) and Fig. 2 (d). Finally the chip was heated at 90 C for 1 min on the manipulator in order to leave the PPC film on the chip, dipped it in chloroform for 10 min to clean the PPC and annealed at 300 C with Ar/H_2 mixing gases for 1 h so as to clean the PPC residues on the encapsulated *h*-BN/graphene/*h*-BN device [7]. On the other hand, the *h*-BN/exfoliated graphene/*h*-BN devices were fabricated with the same transferred method [7]. The *h*-BN/CVD graphene/*h*-BN and *h*-BN/exfolited graphene/*h*-BN devices were measured at room temperature and in low-temperature cryostats using standard ac lock-in techniques.

3. Results and discussion

Fig. 3 (a) shows conductance measurements of the *h*-BN/CVD graphene/*h*-BN device as a function of back gate voltage G (V_{bg}) at room temperature before and after annealing processes that is with Ar/H_2 mixing gases at 300 C. The field-effect mobility μ_{FE} can be calculated by considering the relative permittivities ε in SiO_2 ($\varepsilon = 3.9$, $d = 300$ nm), bottom *h*-BN ($\varepsilon = 4$, $d = 20$ nm) and the suspended space between metal contacts ($\varepsilon = 1$, $d = 55$ nm) as shown

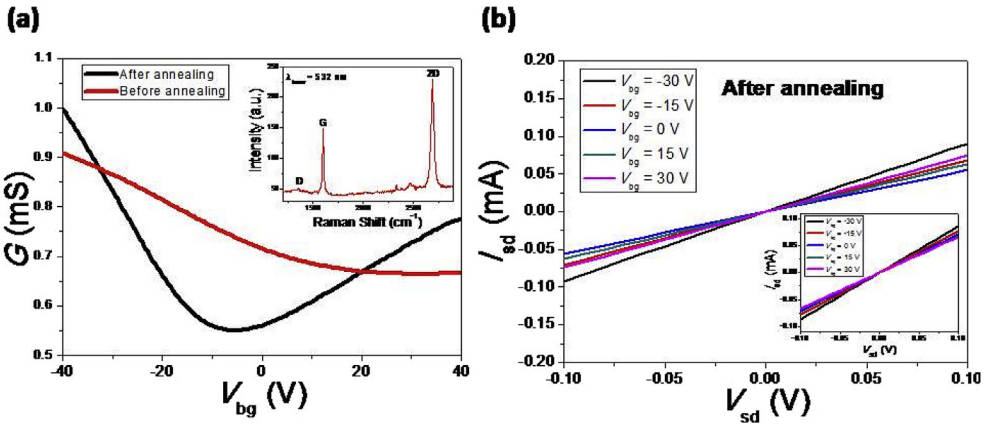

Fig. 3. (a) Conductance as a function of back-gate voltage G (V_{bg}) of the h-BN/CVD graphene/h-BN device for $V_{bg} = -40$ V to 40 V before (red curve) and after (black curve) annealing process at room temperature. The inset shows the Raman spectrum of the CVD graphene on SiO_2 substrate. (b) The I_{sd} (mA) as a function of V_{sd} (V) measurements at various back gate voltages $V_{bg} = -30$ V, −15 V, 0 V, 15 V and 30 V at room temperatures after the annealing process. The inset shows the I_{sd} (mA) as a function of V_{sd} (V) measurements at the same V_{bg} conditions before the annealing process. (A colour version of this figure can be viewed online.)

in Fig. 2 (a) (Ref. 30). Before the annealing processes, the Dirac point is far from zero voltage (> 40 V) and the hole mobility $\mu_{FE} \approx 800\ cm^2/Vs$ is at room temperature due to the p-type chemical doping during optical lithography and CVD graphene transferred processes [34]. After the annealing processes, the Dirac point was around $V_D = -5$ V and the hole mobility $\mu_{FE} \approx 2600\ cm^2/Vs$ and electron mobility $\mu_{FE} \approx 900\ cm^2/Vs$ at room temperature. The electron and hole mobilities are quite different, possibly due to the intrinsic grain boundary characteristics in CVD graphene [35,36]. These results suggest that the annealing processes can effectively improve the transport mobility property in our device due to the suspended space between metal contacts and graphene. Our suspended h-BN/graphene on bottom metal/h-BN can decrease the effect of suspended graphene strain so as to maintain excellent electronic transport property, because the thick (30 nm) and hard top h-BN layer can hold graphene very flat by van der Waals force between top h-BN and graphene [6,37]. More importantly, the annealing process not only effectively clean the polymer residues of graphene, but also decrease the two-terminal resistance of the device (See supplementary materials) [Ref. 38]. The Raman spectra of commercial CVD graphene on SiO_2 were measured using a 532-nm laser as shown in the inset of Fig. 3 (a). The full width at half maximum (FHWM) of the 2D peak is 33 cm^{-1} that is between single layer (35 cm^{-1}) and bilayer (30 cm^{-1}) (Ref. 9), which is consistent with the fact that our graphene is composed 10–30% bilayer islands [32]. The inset of Fig. 3 (b) and Fig. 3 (b) show the current-voltage (I–V) curves at different back gate voltages V_{bg} before and after annealing processes. Both of them reveal excellent Ohmic behaviors and correspond to the resistance value in back gate voltage dependence as shown in Fig. 3 (a), which proves the excellent electronic property during photo-lithography fabrication processes with less chemical bonding to carbon atoms that might cause the insulating property [39–41].

In order to study coherent transport property in such an h-BN/CVD grphene/h-BN device, we performed low-temperature G (V_{bg}) measurements of the device as shown in Fig. 4 (a). The field-effect hole and electron mobilities were $\mu_{FE} \approx 3300\ cm^2/Vs$ and $\mu_{FE} \approx 2400\ cm^2/Vs$, respectively. As we have a two-terminal graphene device, it is not possible to determine the contact resistance. Nevertheless, we have fabricated an eight-terminal h-BN/CVD graphene device which allows us to measure the contact resistance of the device to be 745 Ω (Supplementary information). We estimate that for our two-terminal suspended devices, the contact resistance is of the order of 750 Ω. Clear conductance oscillations from $V_{bg} = -40$ V–40 V at $T = 0.3$ K were observed and were gradually suppressed when temperature was raised to 30 K due to the increased thermal smearing. This result is reminiscent of electric Aharonov-Bohm-like effect [21–23]. Interestingly, the Dirac point near $V_{bg} = -13$ V became wide and was somewhat hard to be located from the conductance oscillations, which was possibly due to the imperfect lattice mismatch from the strain and rotated lattice angle between h-BN and CVD graphene [42,43]. The conductance oscillations from $V_{bg} = -40$ V to 40 V at $T = 0.3$ K can be revealed clearly after filtering the average background as shown in Fig. 4(b) and (c) on both the hole and electron sides. Interestingly, the amplitude of conductance oscillations after filtering the average background in h-BN/single layer exfoliated graphene/h-BN was approximately the same as that in h-BN/CVD graphene/h-BN system [21–23] with $\Delta G \approx 0.1\ e^2/h$ and also approximately one order magnitude larger than that in the commercial CVD graphene/SiO_2 system $\Delta G \approx 0.01\ e^2/h$ (See supplementary materials Fig. S2 (b)) as shown in Fig. 5(c) and (d) on both the hole and electron sides, which further revealed that top and bottom h-BN encapsulated graphene were key factors for the enhancement of interference effect. On the other hand, the insets of Fig. 4(b) and (c) show the period interval in $\Delta V_{bg} = 0.05$ V from the Lorentzian fit to the fast Fourier transform (FFT) spectrum [21,22,44], which further lends support to the existence of electric Aharonov-Bohm-like effect. In Fig. 4 (d), the root mean square conductance amplitude (ΔG_{rms}) extracted from the data taken on the electron side as shown in Fig. 4 (c) at higher temperatures showed a T^{-1} dependence and a saturation at low temperatures that were common characteristics in disordered graphene systems [44,45]. This is vastly different from the $T^{-0.5}$ dependence in CVD graphene/SiO_2 systems (See Supporting Information) [21,22]. Such a difference between $T^{-0.5}$ in CVD graphene/SiO_2 and T^{-1} in CVD graphene/h-BN may suggest that the thermal energy averaging of the h/e oscillations dissipated more quickly in h-BN substrate rather than that on a SiO_2 substrate, which indicates that h-BN is an excellent heat transferring media [25,46,47] for graphene-based interference-type nanodevices [48].

One might be interested in whether the enscapsulated h-BN layer played an important role in the enhancement of intereference effect due to electric Aharonov-Bohm-like effect from the ring trajectory within CVD graphene [22,23]. In order to simulate this situation, we used h-BN/single layer exfoliated graphene/h-BN device in such a fabrication method. Fig. 5 (a) shows the G (V_{bg})

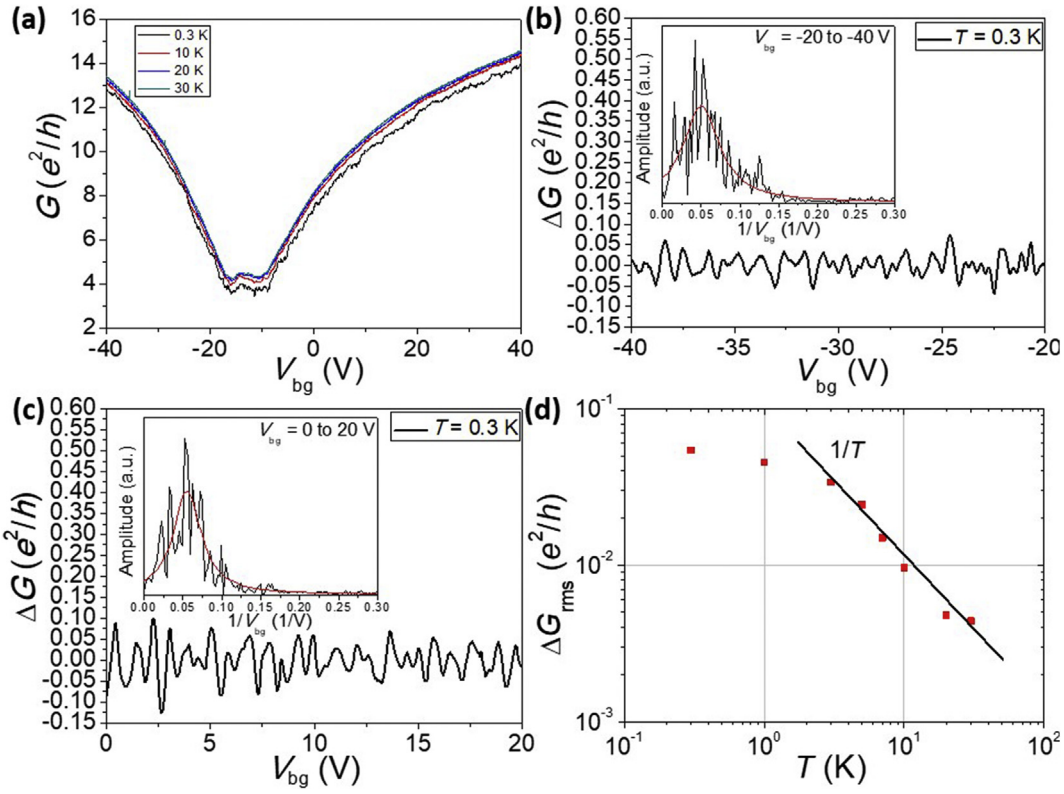

Fig. 4. (a) G (e^2/h) of the h-BN/CVD graphene/h-BN device as a function of V_{bg} from $V_{bg} = -40$ V to 40 V after annealing at $T = 0.3$ K, 10 K, 20 K and 30 K. (b) and (c) The conductance oscillations of the h-BN/CVD graphene/h-BN device at $T = 0.3$ K from $V_{bg} = -20$ V to -40 V and 0 to 20 V on the hole and electron sides after filtering the averaging background. The insets show the FFT spectra of the conductance oscillations with a Lorentzian fit extracted from Fig. 4 (b) and (c). (d) The ΔG_{rms} amplitude extracted from the data on the electron side as Fig. 4 (c) with different temperatures in semi-logarithmic scale. The solid line shows the data in the high temperature regime exhibits a T^{-1}dependence. (A colour version of this figure can be viewed online.)

measurements of an h-BN/single layer exfoliated graphene/h-BN device at room temperatur after annealing processes. The field effect hole and electron mobility are about the same $\mu_{FE} \approx 10000\ cm^2/Vs$. Moreover, the Dirac point is near $V_{bg} = 0$ V, which revealed the excellent transport mobility, pristine graphene property. At $T = 0.3$ K, the conductance oscillated obviously and the field effect hole and electron mobility were $\mu_{FE} \approx 30000\ cm^2/Vs$ symmetrically, which showed the quasi-ballistic transport property in such a device [27,28]. Interestingly, the Dirac point near $V_{bg} = 3.5$ V was not wide in comparision with the h-BN/CVD graphene/h-BN device as shown in Fig. 4 (a), which suggested that the improvement of graphene film quanlity, like much fewer defects, would compensate the graphene linear band completeness rather than that the imperfect lattice mismatch from the rotated lattice angle and strain between h-BN and CVD graphene [42,43]. Interestingly, the amplitude of conductance oscillations after filtering the average background in h-BN/single layer exfoliated graphene/h-BN was approximately the same as that in h-BN/CVD graphene/h-BN system [21–23] and also approximately one order magnitude larger than that in the commercial CVD graphene/SiO_2 system (See supporting information) as shown in Fig. 5 (c) and (d) on both the hole and electron sides, which further revealed that top and bottom h-BN encapsulated graphene were key factors for the enhancement of interference effect. Again, the insets of Fig. 5(c) and (d) reveal the period interval for the hole and electron sides from the Lorentzian fit to the FFT spectrum [21,22,44] which is in line with the electric Aharonov-Bohm-like effect. Our mechanically exfoliated graphene from HOPG may not suffer from small grain size and grain boundaries in graphene. Thus due to disorder interference between phase-coherent electron paths that cross the h-BN/graphene/h-BN device can give rise to conductance fluctuations.

We note that for CVD graphene, the grain sizes are dependent on growth conditions, ranging from hundreds of nanometers to tens of microns for slight changes in growth condition. Although we do not have direct measurements on the average grain size in our CVD-graphene, we believe that it is similar to that reported in CVD graphene transferred onto TEM grids (250 nm) [Ref. 35]. It is believed that intrinsic topological defects of graphene, like grain boundaries [21–23,49,50], dislocations [50,51], kinks [52] and cones [53] may give rise to Aharonov-Bohm-like oscillations in graphene. If we can control the grain boundaries in CVD graphene by seeded growth as proposed by Yu et al. [54], we may deliberately allow the electrons or holes in graphene to go around an intrinsic topological defect like grain boundaries through two arms in a ring-like structure, giving rise to electric Aharonov-Bohm-like oscillations. At present, the coherent transport in our h-BN/CVD-graphene/h-BN device is attributed to disorder-related interference between electron paths that cross the graphene system. We note that the CVD growth method could allow graphene to be grown on h-BN [Refs. 55–57]. Therefore, the interference effect in h-BN/CVD graphene/h-BN prepared by such fabrication method could be further improved, a great potential for industrial scheme applications.

4. Conclusions

We have fabricated h-BN/CVD graphene/h-BN heterostructure device without using high-cost e-beam processes and toxic gas etching. Our device reveals excellent linear Ohmic behavior. Moreover, the amplitude of the conductance oscillations in the h-

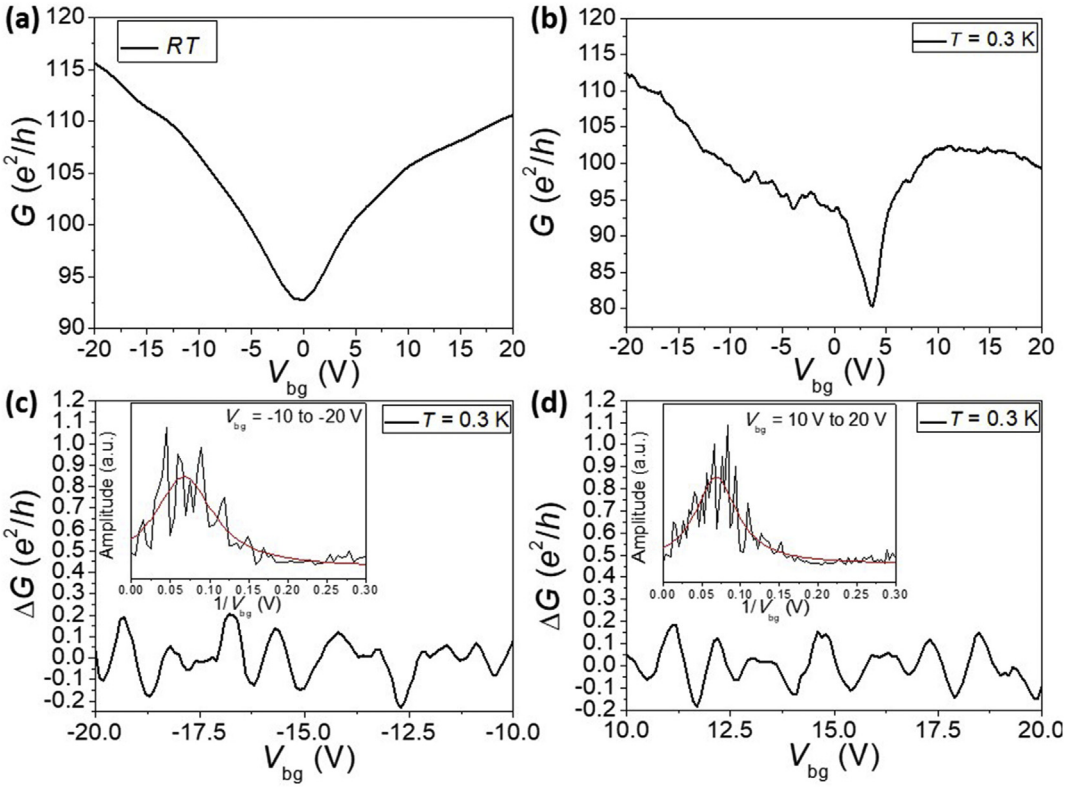

Fig. 5. (a) The conductance in the *h*-BN/exfoliated graphene/*h*-BN device as a function of V_{bg} at room temperature from $V_{bg} = -20$ to 20 V after annealing process. (b) The conductance in the *h*-BN/exfoliated graphene/*h*-BN device as a function of V_{bg} at $T = 0.3$ K from $V_{bg} = -20$ V to 20 V. (c) and (d) The ΔG_{rms} amplitude of the *h*-BN/CVD graphene/*h*-BN device at $T = 0.3$ K from $V_{bg} = -10$ V to -20 V and 10 V to 20 V on the hole and electron sides after filtering the averaging background. The insets show the FFT spectra of the conductance oscillations with a Lorentzian fit extracted on the data on the hole side as Fig. 5(c) and the electron side as Fig. 5(d). (A colour version of this figure can be viewed online.)

BN/graphene/*h*-BN device is an order of magnitude larger than that in the CVD graphene/SiO_2 system and revealed the T^{-1} dependence in root mean square conductance oscillations, which suggested the enhancement of interface effect probably due to the high-quality *h*-BN and graphene interfaces. Such an *h*-BN/CVD graphene/*h*-BN device provides an excellent heat transferring media for graphene-based interference-type electronic devices. We propose that finely controlled grain boundaries of CVD graphene could further enhance the interference effect in our *h*-BN/CVD graphene/*h*-BN device, a great advantage for future low-cost graphene-based interference-type electronic applications.

Acknowledgements

C. C. would like to acknowledge the Ministry of Science and Technology (MOST), Taiwan, for financial support (Grant no. MOST 108-2112-M-033-001- MY3). K. W. and T. T. acknowledge support from the Elemental Strategy Initiative conducted by the MEXT, Japan and the CREST (JPMJCR15F3), JST. C.-T.L. thanks MOST, Taiwan for financial support (Grant no. MOST 105-2112-M-002-005-MY3, MOST 107-2622-8-002 -018), and MOST 107-2627-E-002-002. N. A. thanks funding from JSPS KAKENHI Grant no. 18H01812.

Appendix A. Supplementary data

Supplementary data to this article can be found online at https://doi.org/10.1016/j.carbon.2019.07.057.

References

[1] C. Mattevi, H. Kim, M. Chhowalla, A review of Chemical Vapour deposition of graphene on copper, J. Mater. Chem. 21 (2011) 3324.
[2] Y. Zhang, L. Zhang, C. Zhou, Review of chemical vapor deposition of graphene and related applications, Acc. Chem. Res. 46 (2013) 2329.
[3] A.N. Obraztsov, Making graphene on a large scale, Nat. Nanotechnol. 4 (2009) 212.
[4] K.S. Kim, Y. Zhao, H. Jane, S.Y. Lee, J.M. Kim, K.S. Kim, et al., Large-scale pattern growth of graphene films for stretchable transparent electrodes, Nature 457 (2009) 706.
[5] X. Li, W. Cai, J. An, S. Kim, J. Nah, D. Yang, et al., Large-area synthesis of high-quality and uniform graphene films on copper foils, Science 324 (2009) 1312.
[6] C.R. Dean, A.F. Young, I. Meric, C. Lee, L. Wang, S. Sorgenfrei, et al., Boron nitride substrates for high-quality graphene electronics, Nat. Nanotechnol. 5 (2010) 722.
[7] L. Wang, I. Meric, P.Y. Huang, Q. Gao, Y. Gao, H. Tran, et al., One-dimensional electrical contact to a two-dimensional material, Science 342 (2013) 614.
[8] H. Wang, T. Taychatanapat, A. Hsu, K. Watanabe, T. Taniguchi, P. Jarillo-Herrero, et al., BN/Graphene/BN transistors for RF applications, IEEE Electron. Device Lett. 32 (2011) 1209.
[9] A. Reina, X. Jia, J. Ho, D. Nezich, H. Son, V. Bulovic, et al., Large area, few-layer graphene films on arbitrary substrates by chemical vapor deposition, Nano Lett. 9 (2009) 30.
[10] N. Petrone, C.R. Dean, I. Meric, A.M. van der Zande, P.Y. Huang, L. Wang, et al., Chemical vapor deposition-derived graphene with electrical performance of exfoliated graphene, Nano Lett. 12 (2012) 2751.
[11] V.E. Calado, S.-E. Zhu, S. Goswami, Q. Xu, K. Watanabe, T. Taniguchi, et al., Ballistic transport in graphene grown by chemical vapor deposition, Appl. Phys. Lett. 104 (2014), 023103.
[12] L. Banszerus, M. Schmitz, S. Engels, M. Goldsche, K. Watanabe, T. Taniguchi, et al., Ballistic transport exceeding 28 μm in CVD grown graphene, Nano Lett. 16 (2016) 1387.
[13] W. Gannett, W. Regan, K. Watanabe, T. Taniguchi, M.F. Crommie, et al., Boron nitride substrates for high mobility chemical vapor deposited graphene, Appl. Phys. Lett. 98 (2011) 242105.
[14] J. Baringhaus, M. Ruan, F. Edler, A. Tejeda, M. Sicot, A.T. Ibrahimi, et al., Exceptional ballistic transport in epitaxial graphene nanoribbons, Nature 506

(2014) 349.
[15] V.V. Cheianov, V. Fal'ko, B.L. Altshuler, The focusing of electron flow and a Veselago lens in graphene p-n junctions, Science 315 (2007) 1252.
[16] Q. Wilmart, S. Berrada, D. Torrin, V.H. Nguyen, G. Feve, J.-M. Berroir, et al., A Klein-tunneling transistor with ballistic graphene, 2D Mater. 1 (2014), 011006.
[17] A.K. Singh, G. Auton, E. Hill, A. Song, Graphene based ballistic rectifiers, Carbon 84 (2015) 124.
[18] F. Miao, S. Wijeratne, Y. Zhang, U.C. Coskun, W. Bao, C.N. Lau, Phase-coherent transport in graphene quantum billiards, Science 317 (2007) 1530.
[19] P. Rickhaus, R. Maurand, M. Liu, M. Weiss, K. Richter, C. Schönenberger, Snake trajectories in ultraclean graphene p-n junctions, Nat. Commun. 4 (2014) 2342.
[20] T. Taychatanapat, K. Watanabe, T. Taniguchi, P. Jarillo-Herrero, Electrically tunable transverse magnetic focusing in graphene, Nat. Phys. 9 (2013) 225.
[21] C. Chuang, M. Matsunaga, F.-H. Liu, T.-P. Woo, N. Aoki, L.-H. Lin, et al., Probing weak localization in chemical vapor deposition graphene wide constriction using scanning gate microscopy, Nanotechnology 27 (2016), 075601.
[22] C. Chuang, M. Matsunaga, F.-H. Liu, T.-P. Woo, L.-H. Lin, K. Oto, et al., Imaging coherent transport in chemical vapor deposition graphene wide constriction by scanning gate microscopy, Appl. Phys. Lett. 108 (2016) 123105.
[23] C. Chuang, T.-P. Woo, F.-H. Liu, M. Matsunaga, Y. Ochiai, N. Aoki, et al., High current-induced electron redistribution in a CVD-grown graphene wide constriction, J. Nanomater. 2016 (2016) 1806871.
[24] J. Munárriz, F. Domínguez-Adame, A.V. Malyshev, Toward graphene-based quantum interference devices, Nanotechnology 22 (2011) 365201.
[25] C. Chuang, M. Mineharu, N. Matsumoto, M. Matsunaga, C.-W. Liu, B.Y. Wu, et al., Hot carriers in CVD-grown graphene device with a top *h*-BN layer, J. Nanomater. 2018 (2018) 5174103.
[26] C. Chuang, C.-T. Liang, G.-H. Kim, R.E. Elmquist, Y. Yang, Y.P. Hsieh, et al., Large, non-saturating magnetoresistance in single layer chemical vapor deposition graphene with an *h*-BN capping layer, Carbon 136 (2018) 211.
[27] C.R. da Cunha, M. Mineharu, M. Matsunaga, N. Matsumoto, C. Chuang, Y. Ochiai, et al., Conductance fluctuations in high mobility monolayer graphene: nonergodicity, lack of determinism and chaotic behavior, Sci. Rep. 6 (2016) 33118.
[28] N. Matsumoto, M. Mineharu, M. Matsunaga, C. Chuang, Y. Ochiai, K. Oto, et al., Shubnikov-de Haas measurements on a high mobility monolayer graphene flake sandwiched between boron nitride sheets, J. Phys. Condens. Matter 29 (2017) 225301.
[29] K. Watanabe, T. Taniguchi, H. Kanda, Direct-bandgap properties and evidence for ultraviolet lasing of hexagonal boron nitride single crystal, Nat. Mater. 3 (2004) 404.
[30] K.S. Novoselov, A.K. Geim, S.V. Morozov, D. Jiang, Y. Zhang, S.V. Dubonos, et al., Electric field effect in atomically thin carbon films, Science 306 (2004) 666.
[31] C. Kumar, M. Kuiri, J. Jung, T. Das, Anindya Das, Tunability of 1/f noise at multiple Dirac cones in hBN encapsulated graphene devices, Nano Lett. 16 (2016) 1042.
[32] (Website), https://graphene-supermarket.com/CVD-Graphene-on-SiO2-Si/.
[33] A. Castellanos-Gomez, M. Buscema, R. Molenaar, V. Singh, L. Janssen, H.S.J. van der Zant, et al., Deterministic transfer of two-dimensional materials by all-dry viscoelastic stamping, 2D Mater. 1 (2014), 011002.
[34] F. Schedin, A.K. Geim, S.V. Morozov, E.W. Hill, P. Blake, M.I. Katsnelson, et al., Detection of individual gas molecules adsorbed on graphene, Nat. Mater. 6 (2007) 652.
[35] P.Y. Huang, C.S. Ruiz-Vargas, A.M. van der Zande, W.S. Whitney, M.P. Levendorf, J.W. Kevek, et al., Grains and grain boundaries in single-layer graphene atomic patchwork quilts, Nature 469 (2011) 389.
[36] X.S. Li, C.W. Magnuson, A. Venugopal, J.H. An, J.W. Suk, B.Y. Han, et al., Graphene films with large domain size by a two-step chemical vapor deposition process, Nano Lett. 10 (2010) 4328.
[37] H. Zhang, J.-W. Huang, J.V. Jr., J. Myhro, M. Maldonado, D.D. Tran, et al., Transport in suspended monolayer and bilayer under stain: a new platform for material study, Carbon 69 (2014) 336.
[38] O. Balci, K. Kocabas, Appl. Phys. Lett. 101 (2012) 243105.
[39] C. Chuang, R.K. Puddy, H.-D. Lin, S.-T. Lo, T.-M. Chen, C.G. Smith, et al., Experimental evidence for Efros-Shklovskii variable range hopping in hydrogenate graphene, Solid State Commun. 152 (2012) 905.
[40] C. Chuang, R.K. Puddy, M.R. Connolly, S.-T. Lo, H.-D. Lin, T.-M. Chen, et al., Evidence for formation of multi-quantum dots in hydrogenated graphene, Nanoscale Res. Lett. 7 (2012) 459.
[41] S.-T. Lo, C. Chuang, R.K. Puddy, T.-M. Chen, C.G. Smith, C.-T. Liang, Non-ohmic behavior of carrier transport in highly disordered graphene, Nanotechnology 24 (2013) 165201.
[42] Z.H. Ni, T. Yu, Y.H. Lu, Y.Y. Wang, Y.P. Feng, Z.X. Shen, Uniaxial strain on graphene: Raman Spectroscopy study and band-gap opening, ACS Nano 2 (2008) 2301.
[43] E. Suárez Morell, P. Vargas, L. Chico, L. Brey, Charge redistribution and interlayer coupling in twisted bilayer graphene under electric fields, Phys. Rev. B 84 (2011) 195421.
[44] M. Huefner, F. Molitor, A. Jacobsen, A. Pioda, C. Stampfer, K. Ensslin, et al., The Aharonov-Bohm effect in a side-gated graphene ring, New J. Phys. 12 (2010), 043054.
[45] C. Chuang, L.-H. Lin, N. Aoki, T. Ouchi, A.M. Mahjoub, T.-P. Woo, et al., Mesoscopic conductance fluctuations in multi-layer graphene, Appl. Phys. Lett. 103 (2013), 043117.
[46] M.-H. Tsai, I.-H. Tseng, J.-C. Chiang, J.-J. Li, Flexible polyimide films hybrid with functionalized boron nitride and graphene oxide simultaneously to improve thermal conduction and dimensional stability, ACS Appl. Mater. Interfaces 6 (2014) 8639.
[47] N. Sakhavand, R. Shahsavari, Dimensional crossover of thermal transport in hybrid boron nitride nanostructures, ACS Appl. Mater. Interfaces 7 (2015) 18312.
[48] A.C. Betz, S.H. Jhang, E. Pallecchi, R. Ferreira, G. Fève, J.-M. Berroir, et al., Supercollision cooling in undoped graphene, Nat. Phys. 9 (2013) 109.
[49] A. Mesaros, S. Papanilkolaou, C.F.J. Flipse, D. Sadri, J. Zaane, Electronic states of graphene grain boundaries, Phys. Rev. B 82 (2019) 205119.
[50] F. Gargiulo, Oleg V. Yazyev, Topological aspects of charge-carrier transmission across grain boundaries in graphene, Nano Lett. 14 (2014) 250.
[51] A. Measaros, D. Sadri, J. Zaanen, Berry phase of dislocations in graphene and valley conserving decoherence, Phys. Rev. B 79 (2009) 155111.
[52] L.J.P. Xavier, J.M. Pereira Jr., Andrey Caves, G.A. Farias, F.M. Peeters, Topological confinement in graphene bilayer quantum rings, Appl. Phys. Lett. 96 (2010) 212108.
[53] P.E. Lammert, V.H. Crespi, Topological phases in graphitic cones, Phys. Rev. Lett. 85 (2000) 5190.
[54] Q. Yu, L.A. Jauregui, W. Wu, R. Colby, J. Tian, Z. Su, et al., Control and characterization of individual grains and grain boundaries in graphene grown by chemical vapour deposition, Nat. Mater. 10 (2011) 443.
[55] N. Mishra, V. Miseikis, D. Convertino, M. Gemmi, V. Piazza, C. Coletti, Rapid and catalyst-free van der Waals epitaxy of graphene on hexagonal boron nitride, Carbon 96 (2016) 497.
[56] S. Tang, G. Ding, X. Xie, J. Chen, C. Wang, X. Ding, et al., Nucleation and growth of single crystal graphene on hexagonal boron nitride, Carbon 50 (2012) 329.
[57] X. Ding, G. Ding, X. Xie, F. Huang, M. Jiang, Direct growth of few layer graphene on hexagonal boron nitride by chemical vapor deposition, Carbon 49 (2011) 2522.